Journal of Geochemical Exploration 199 (2019) 1–15

Contents lists available at ScienceDirect

Journal of Geochemical Exploration

journal homepage: www.elsevier.com/locate/gexplo

Tectonic setting and mineralization potential of the Zefreh porphyry Cu-Mo deposit, central Iran: Constraints from petrographic and geochemical data

Maryam Khosravi[a], Mohammad Ali Rajabzadeh[a,*], KeZhang Qin[b,c], Hooshang H. Asadi[d]

[a] Department of Earth Sciences, Faculty of Sciences, Shiraz University, Shiraz, Iran
[b] Key Laboratory of Mineral Resources, Institute of Geology and Geophysics, Chinese Academy of Sciences, Beijing 100029, China
[c] University of Chinese Academy of Sciences, Beijing 100049, China
[d] Department of Mining Engineering, Isfahan University of Technology, Isfahan 8415683111, Iran

ARTICLE INFO

Keywords:
Zefreh porphyry Cu-Mo deposit
Normal calc-alkaline magma
Geochemistry
Petrography
Tectonics

ABSTRACT

The Zefreh porphyry Cu-Mo deposit is located in the central part of the Cenozoic Urumieh-Dokhtar Magmatic Arc (UDMA), 75 km NE of Isfahan city, central Iran. The Zefreh rocks, ranging from diorite to granodiorite in composition, formed in a subduction-related arc setting, and likely in a pre-plate collisional environment. They are enriched in Th, U, Rb, Pb, light rare earth elements (LREE), but depleted in Ti, Nb, Ta, Ba, Sr, and P. Negative to slightly positive Eu anomalies (0.5–1.1), low to moderate Sr contents, (189–567 ppm), low to moderate Sr/Y ratios (5–23), and low La/Yb ratios (3–8) in the Zefreh magmatic suite rule out considerable amounts of fractionated amphibole from a hydrous magma in the lower crust. Arc crustal thickness in the Zefreh area was probably < 40 km at the time of emplacement of the granitoids, under which amphibole did not fractionate considerably from the primitive magma. Melting of garnet-free lower-crustal amphibolites, together with fractional crystallization and crustal assimilation processes may be the main source of the Zefreh granitoids. On the basis of geochemical characteristics of the granitoids (e.g., low to moderate Sr contents, moderate to high contents of Y and Yb, low to moderate ratios of Sr/Y and Dy/Yb, low La/Yb ratios, negative to slightly positive Eu anomalies, and negative anomalies of Sr) and immature arc with thin crust, the Zefreh deposit is likely to be a small, sub-economic porphyry Cu-Mo deposit.

1. Introduction

Porphyry Cu-Mo-Au deposits (hereafter, PCDs) are usually associated with subduction-related magmas. They can be found in different tectonic settings, including continental arcs (e.g., Andes, North American Cordillera; Sillitoe, 1972; Shafiei et al., 2009, and references therein, North Tibet of China, and Central Asian Orogenic Belt; Qin, 2012), syn- to post-collisional orogenic belts (e.g., western Asia; Shafiei et al., 2009, and southern Tibet; Hou et al., 2015), and pre-collisional back-arcs (e.g., East Central Anatolia, Turkey; Richards, 2015, and southern Tibet; Li et al., 2011). Their formation is generally attributed to separation of metalliferous and sulfur-rich hydrothermal fluids from calc-alkaline magmas (Sillitoe, 2010). Richards and Kerrich (2007) argued that the most sulfur-rich and oxidized subduction-related arc magmas have the highest potential to form large porphyry deposits, and that these include adakites, defined by high Sr/Y and La/Yb ratios, along with low Y and Yb contents. These geochemical features of the adakitic magmas are attributed to fractionation of amphibole and/or garnet from the primitive magma (Defant and Drummond, 1990; Martin, 1999). There is also a close connection, frequently noted, between the maturity of arc magmatism and the development of porphyry deposits during the syn- to post-collisional stages of orogenesis (e.g., Shafiei et al., 2009; Richards et al., 2012; Asadi et al., 2014).

The geology of western Iran is divided into three parallel, NW-trending belts: (1) the Urumieh-Dokhtar Magmatic Arc (UDMA), (2) the Sanandaj-Sirjan Metamorphic Zone (SSMZ), (3) the Zagros Fold and Thrust Belt (ZFTB) (Fig. 1). PCDs in western Iran are restricted to the UDMA. The main copper-bearing metallogenic belt of the UDMA has been divided along strike into northwest, central, and southeast segments (Chiu et al., 2013), hereafter referred to as the Arasbaran Magmatic Arc (AMA), Saveh-Yazd Magmatic Arc (SYMA), and Kerman Cenozoic Magmatic Arc (KCMA), respectively. Well-known PCDs include the Sar-Cheshmeh and Meiduk deposits in the KCMA, and the Sungun deposit in the AMA (Fig. 1). Geochemical studies of magmatic rocks associated with PCDs, especially the trace elements and Rare Earth Elements (REE), often provide essential constraints in

* Corresponding author.
E-mail addresses: mrajabzadeh@shirazu.ac.ir, rajabzad@susc.ac.ir (M.A. Rajabzadeh).

https://doi.org/10.1016/j.gexplo.2019.01.001
Received 22 September 2018; Received in revised form 7 January 2019; Accepted 13 January 2019
Available online 15 January 2019
0375-6742/

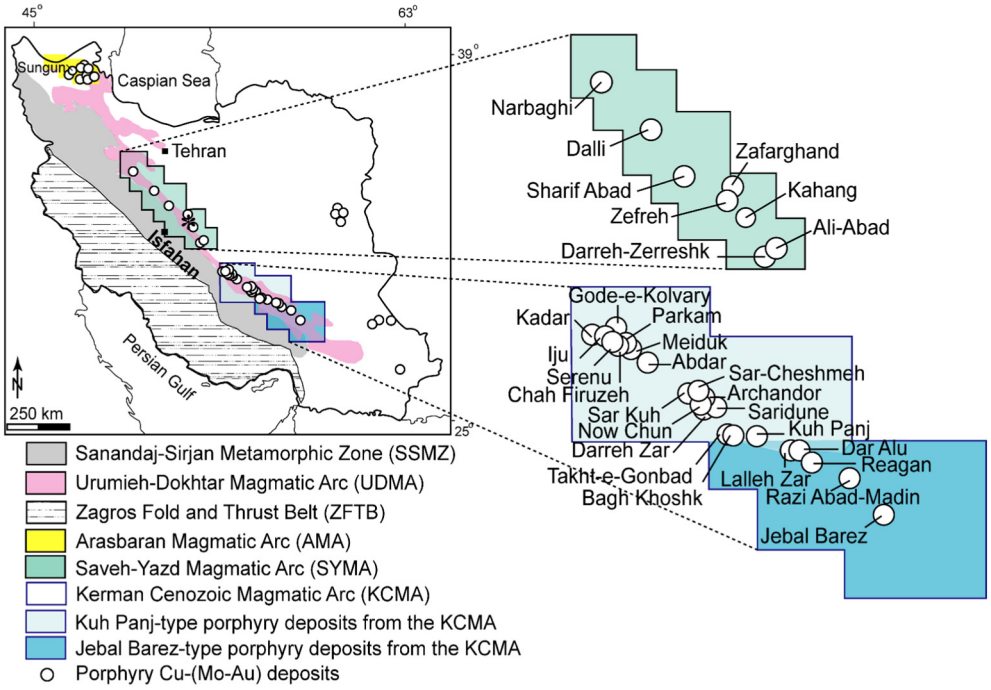

Fig. 1. Zonal subdivisions of the Zagros orogen (Ghasemi and Talbot, 2006); inset shows location of the Zefreh deposit and other major porphyry Cu-(Mo-Au) deposits along the UDMA.

constructing geologic, magmatic, and geodynamic models for the evolution of the deposit. In this regard, for the KCMA in central Iran, magmatic evolution from the normal calc-alkaline (Jebal Barez-type) in the Late Eocene, to the adakitic signature (Kuh Panj-type) in the Middle to Late Miocene was attributed to evolution of the magmatic arc system and arc crustal thickening during the Alpine-Himalayan orogeny (Shafiei et al., 2009; Asadi et al., 2014). Furthermore, geochemical data from intrusive rocks of central and eastern Iran, and western Pakistan indicated that arc crustal thickening, together with high magmatic water content in the more evolved magmas, resulted in the development of fertile magmatic-hydrothermal (porphyry) deposits (Richards et al., 2012). In the KCMA, the Late Eocene calc-alkaline intrusions of the Jebal Barez-type led to the earliest, typically small and barren porphyry deposits. Whereas, the Middle-to-Late Miocene dioritic to granodioritic intrusions of the Kuh Panj-type heralded the main period of mineralization, host high-grade and economic porphyry deposits (Shafiei et al., 2009; Asadi et al., 2014).

Within the SYMA segment, there are a large number of discontinuous copper ore bodies of variable sizes. They include the Dalli, Kahang, Zafarghand, Ali Abad, Darreh-Zerreshk, Narbaghi, Sharif Abad, and Zefreh porphyry deposits (Fig. 1). Despite the scientific and economic importance of these deposits in the SYMA, there have been few studies, and no consensus on a petrogenetic model for porphyry mineralization in this region has been developed.

The Zefreh deposit is a porphyry Cu-Mo deposit in the SYMA, and is currently being explored. This deposit and alteration zones were detected, through the multispectral satellite images by Dorsa Pardaze Company in 2012. Furthermore, mapping of iron oxides/hydroxides of this porphyry deposit, using Worldview-3 VNIR data was conducted by Salehi and Tangestani (2018). Mapping, geochemical sampling (259 rock samples from surface), geophysical surveying, and drill core logging were also performed by Dorsa Pardaze Company in order to locate mineralization and zones of alteration, and to determine the relative timing of magmatism and mineralizing events. Lithologic contacts and elemental concentrations of the altered samples were mapped at 1:5000 scale. Ultimately, three favorable locations in the northern, eastern, and southern parts of the deposit were identified by geochemical sampling during preliminary exploration. Thus far, 3 bore holes (totally 553 m long) have been defined an ore body, with a reserve estimation of 1,237,600 tons of sulfide copper ore, with an average grade of 0.34% Cu (Dorsa Pardaze, 2012). We present the first petrologic and geochemical studies of igneous rocks associated with porphyry Cu-Mo mineralization in the Zefreh area. We have used the geochemical and tectonomagmatic characteristics of the Zefreh rocks, and those of the representative granitoid rocks in the SYMA, and also in the KCMA in order to construct economic potential and a petrogenetic model. The reference magmatic suite in the SYMA includes the Ardestan, Zafarghand, and Dalli intrusions, and in the KCMA includes barren (normal calc-alkaline) Jebal Barez-type (e.g., Reagan, Dar Alu, Archandor, and Bagh Khoshk) and economic to sub-economic (adakite-like) Kuh Panj-type (e.g., Sar-Cheshmeh, Meiduk, Darreh Zar, Abdar, Iju, Kader, Chah Firuzeh, Saridune, and Parkam) granitoids (Fig. 1).

2. Regional geology

2.1. General overview

The Zefreh porphyry deposit is located about 75 km NE of Isfahan city in the western part of central Iran in the SYMA of the UDMA (Fig. 1). The UDMA, a NW-trending belt ~2000 km long and 5–25 km wide, is an integral part of the Zagros orogenic belt, the result of convergence between the Arabian plate and the Central Iranian microcontinent (e.g., Berberian et al., 1982; Ghasemi and Talbot, 2006). As an Andean-type subduction-related magmatic arc, the UDMA is mainly composed of voluminous volcanic successions (basalt, basaltic andesite, andesite, dacite, latite, rhyolite, felsic to intermediate tuff, agglomerate, and ignimbrite) and minor (mafic to intermediate and felsic) intrusive rocks (Chiu et al., 2013). Peak magmatism in the UDMA is assigned to the Early Eocene (Ahmadian et al., 2009), the Middle Eocene (Mohajjel et al., 2003), the Oligocene-Middle Miocene (Omrani et al., 2008; Ghorbani et al., 2014), and even Late Miocene (Shahabpour, 2005). In the SYMA, the U-Pb zircon ages for 25 igneous rocks reveal magmatic age dominantly of the Late Paleocene to the Middle Miocene (57-16 Ma; Chiu et al., 2013). Potassium-Ar dating on 6 representative samples of

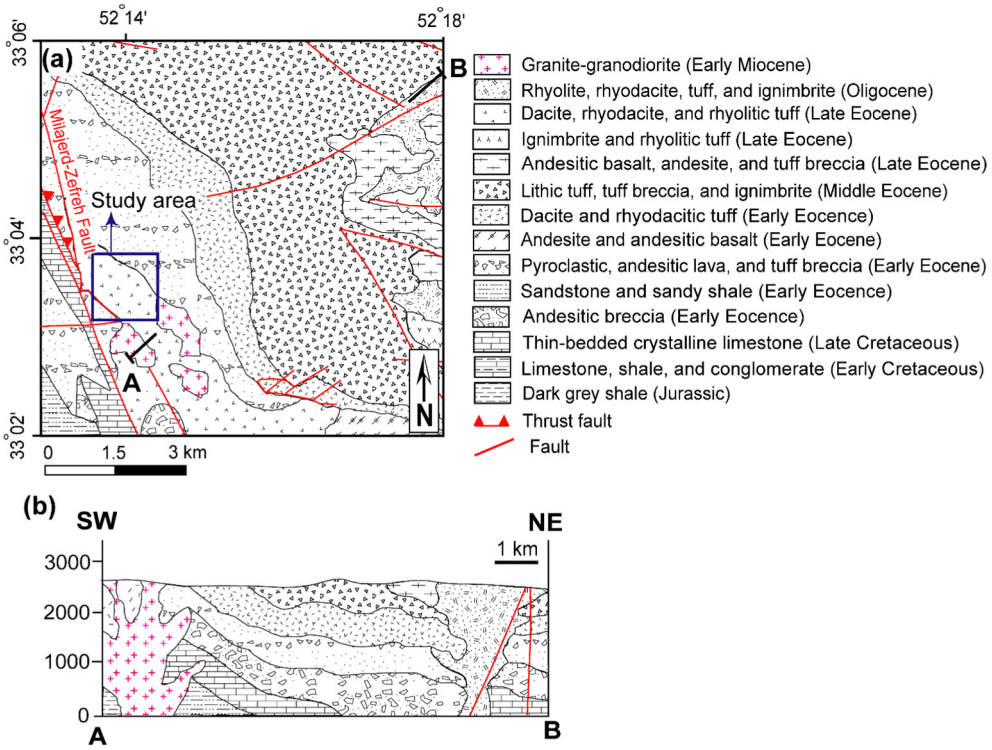

Fig. 2. (a) Simplified geological map showing the local geological setting and lithological units for the Zefreh porphyry Cu-Mo deposit (after Radfar et al., 1999). (b) Cross section illustrates the relationship of plutonic and volcanic units at the regional scale (after Radfar et al., 1999).

igneous rocks in the SYMA by Ghorbani et al. (2014) yielded the Oligocene to the Middle Miocene ages.

2.2. Geological setting

Volcanic activity in the Zefreh area started in the Early Eocene, peaked in the Late Eocene (Fig. 2a; Radfar et al., 1999), and culminated in the Early Miocene (Fig. 3a; Dorsa Pardaze, 2012). The most common rocks are pyroclastic, andesitic lava, and dacite. Based on the regional crosscutting field relationships, pyroclastic and andesitic lava are the oldest lithologic units, making up 30% of the surface exposures in the study area. These rocks lie in the peripheral parts of the deposit in the NNE and SSW parts of the area (Fig. 3a). Dacite dominates the central parts of the deposit, making up > 60% of the rock units. The dacitic unit was affected by phyllic and argillic alterations (Fig. 3b). The subvolcanic intrusive rocks in the Zefreh area are classified into two main groups: granodiorite porphyry and granite porphyry. The former occurs, sometimes as discrete cone-shaped stocks, in the northern, eastern, and northwestern parts of the deposit. The Eocene volcanic rocks (dacite, pyroclastic, and andesitic lava) form the country rocks of the granodioritic stock, and this stock intruded into these volcanic rocks (Fig. 4a). The granodioritic stock is weakly altered, constituting the highest mountains in the study area. Contacts between the porphyry stock and the volcanic rocks are relatively discriminable; however, discriminating the granodiorite porphyry from the granite porphyry is difficult in the field, because of the same color appearance. Subsequent to emplacement, the igneous rocks and surrounding Eocene volcanic rocks were affected by hydrothermal-magmatic fluids, resulting in the development of hydrothermal alteration zones, cropped out on an area of 1.5 × 1.5 km.

3. Analytical methods

In the Zefreh deposit, > 200 samples were collected from bore holes and surface exposures. Microscopic studies were performed on thin and polished thin sections, and used to guide the selection of samples for further geochemical study. Major oxide abundances for 19 samples were obtained, using X-ray fluorescence spectrometry (XRF) on fused glass disks, using a Phillips PW 2404 instrument at the Analytical Laboratory, Beijing Research Institute of Uranium Geology, China. In this regard, precisions are ± 1–3% relative for elements present in concentrations > 1.0 wt%, and about ± 10% relative for elements present in concentrations < 1.0 wt%. Trace element concentrations of these samples were determined by ICP-MS. Precisions are generally better than 5% for most elements based on replicate analyses of rock standards. In addition, major and trace element concentrations of 8 samples were determined, using a Rigaku Primus X-ray fluorescence spectrometer at Brigham Young University, Provo, United States.

4. Results

4.1. Petrography

Granodiorites consist of quartz (45–50%), plagioclase (25–35%), K-feldspar (5–10%), amphibole (5–8%), and biotite (< 3%) with a porphyritic texture (Fig. 4b). Plagioclase occurs as tabular, euhedral to subhedral phenocrysts up to 4–5 mm in the longest dimension, displaying normal and oscillatory zoning, and often polysynthetic twinning. Amphibole is the most frequent mafic constituent, commonly found as euhedral to subhedral phenocrysts. Zircon, apatite, and opaques are common accessory minerals. The groundmass is fine-grained quartz and K-feldspar. The granite with porphyry texture has the same minerals as the granodiorite, but in different proportions. The granodioritic samples can be discriminated from the granitic samples by an increase in amounts of plagioclase rather than K-feldspar. The dacite has an aphanitic to porphyritic texture, and consists of quartz (up to 60%), K-feldspar (5–10%), and plagioclase (30–35%), with minor mafic minerals (< 5%). In the porphyritic dacitic samples, plagioclase crystals occur as euhedral to subhedral phenocrysts, and often show polysynthetic twinning. In some places, quartz phenocrysts with rounded to

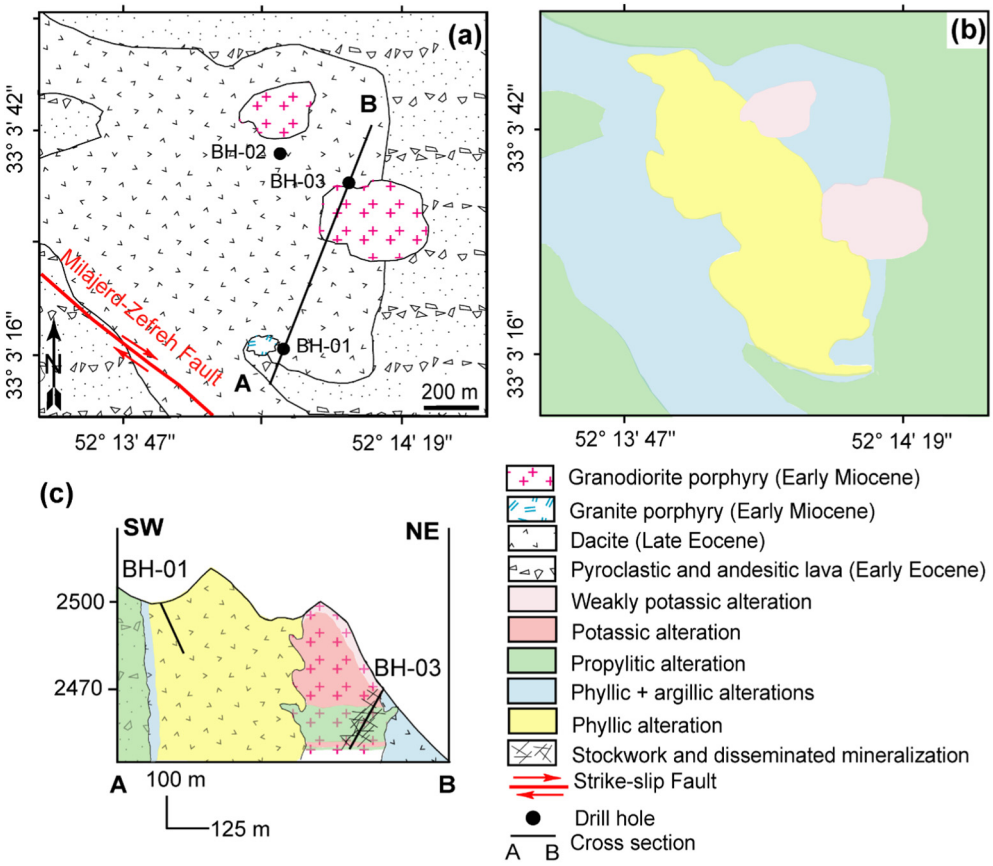

Fig. 3. 1:5000 simplified geological map (a) and alteration map (b) for the Zefreh porphyry Cu-Mo deposit (refer to Fig. 2a for the position of the study area; modified after Dorsa Pardaze, 2012). (c) Schematic cross section showing relative distribution of the alteration zones in the Zefreh porphyry deposit.

sub-rounded and amoeboid shapes are found in an aplitic groundmass of the dacite (Fig. 4c). Andesite with an aphyric texture mainly consists of plagioclase laths (85–90%) and hornblende (5–7%), with minor quartz (< 3%) (Fig. 4d).

4.2. Alteration, mineralization, and vein types

Hydrothermal alterations in the Zefreh area proceed through the propylitic, argillic, phyllic, and potassic alteration zones around the magmatic center. Goethite, hematite, limonite, jarosite, and rare malachite plus azurite are the most common Fe- and Cu-secondary minerals in the surface, due to oxidation of sulfide minerals. The alteration

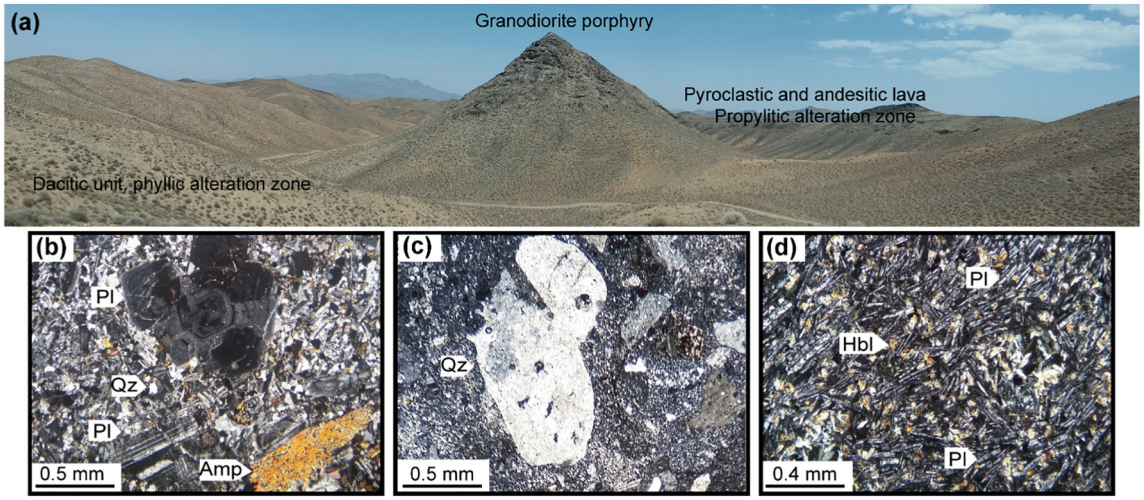

Fig. 4. (a) Intrusion of the porphyritic granodiorite into the volcanic rocks (dacite, pyroclastic, and andesitic lava; looking to the east). Photomicrographs of (b) the granodioritic rock with a porphyritic texture showing quartz, plagioclase, and amphibole (XPL), (c) an amoeboid quartz phenocryst in the dacitic rock (XPL), and (d) plagioclase and hornblende in the andesitic rock (XPL). Mineral abbreviations follow Whitney and Evans (2010). Amp = amphibole, Bn = bornite, Bt = biotite, Cal = calcite, Ccp = chalcopyrite, Chl = chlorite, Cpx = clinopyroxene, Ep = epidote, Grt = garnet, Hbl = hornblende, Kfs = K-feldspar, Mag = magnetite, Mol = molybdenite, Pl = plagioclase, Py = pyrite, Qz = quartz, Ser = sericite, Zrn = zircon.

zones in the Zefreh deposit can be temporally and spatially divided into early, middle, and late stages of alteration. The early stage is characterized by the weakly developed potassic and propylitic alteration zones, generally associated with sulfide-free and sulfide-bearing quartz veins. In the middle stage, the dacite in the center of the mineralized system displays the phyllic and argillic alteration zones. Finally, in the late stage of alteration, the propylitic zone occurs in the peripheral parts of the deposit (Fig. 3b). On the basis of relative abundance of biotite and K-feldspar, the potassic alteration zone is divided into the K-feldspar and biotitic alteration subzones. Also, the propylitic alteration zone can be divided into two subzones, on the basis of sulfide assemblage in drill cores. Pyrite is the only sulfide mineral in the shallower parts of drill cores, whereas chalcopyrite and (sparse) molybdenite occur in the deeper parts of drill cores, adjacent to the potassic alteration zone. As some other well-known PCDs in the UDMA, mineralization commonly occurs in the host rock, and also in the surrounding volcanic rocks (e.g., Shafiei et al., 2009; Asadi et al., 2014; Aminoroayaei Yamini et al., 2017), in the potassic and propylitic alteration zones, and, to a lesser extent, in the phyllic alteration zone. Sulfide minerals are mostly disseminated in the groundmass of the host rock, and also in the quartz-dominated stockwork veins. The dominant sulfide minerals in the hypogene zone are pyrite and chalcopyrite, with molybdenite, and lesser amounts of bornite and chalcocite.

Veins found in each alteration have been classified, on the basis of mineralogy, width of vein, sulfide assemblage, and style of mineralization. Following classification of the veins by Gustafson and Hunt (1975) and Sillitoe (2010), veins in the Zefreh porphyry Cu-Mo deposit are classified into A- and B-type veins (Fig. 5a and b). The A-type veins can be divided into the A_1- and A_2-type veins. The A_1-type veins are dominated by quartz and magnetite, with lesser amounts of chalcopyrite and chlorite, and are generally observed in the K-feldspar alteration subzone. Whereas, the A_2-type veins are characterized by quartz, chalcopyrite, and pyrite, and trace to minor chlorite and epidote, and occur in the potassic and inner propylitic alteration zones. The B-type veins are the most abundant vein type in the altered rocks at Zefreh. These veins are observed in the K-feldspar and inner propylitic alterations, and consist of quartz, pyrite, chalcopyrite, and molybdenite, with lesser amounts of chlorite, epidote, sericite, and calcite. In addition, there are a series of late veinlets devoid of ore minerals (Fig. 5b), and are generally found in all hydrothermal alteration zones, except for the K-feldspar alteration subzone. A summary of the petrographic observations of the alteration zones and vein types is presented in Table 1. The following paragraphs describe the different types of alteration in the Zefreh porphyry Cu-Mo deposit in detail.

4.2.1. Potassic alteration

4.2.1.1. K-feldspar alteration. The K-feldspar alteration zone is generally restricted to the porphyritic granodiorite. Quartz, K-feldspar, and biotite, with lesser amounts of magnetite, chlorite, and epidote are the common alteration minerals of the K-feldspar alteration assemblage, which occur within a fine-grained groundmass in the porphyritic granodiorite (Fig. 6a). This zone is mainly dominated by quartz-rich veins containing pyrite, chalcopyrite, molybdenite, and lesser chlorite and epidote (Fig. 6b). Surrounding of these stockwork veins is a narrow alteration halo of fine-grained sugary quartz and K-feldspar. Disseminated sulfide minerals, whether in the host rocks or the quartz-dominated vein stockworks, make up at most 4 vol% of the altered rocks.

4.2.1.2. Biotitic alteration. Considering the mineral assemblage of alteration, biotite-dominated alteration subzone is similar to the K-feldspar alteration subzone, but pervasive flaky hydrothermal biotite (30–35%) is diagnostic (Fig. 6c). This zone was observed in drill cores through the porphyritic granodiorite, giving hand specimens a typically reddish brown to purple or red tint. Under cross polarized light, hydrothermal biotites vary from greenish brown, through light brown, to brown in color. The hydrothermal biotite replacing the primary mafic minerals forms both fine-grained scaly aggregates (80%) and disseminated flakes (20%) in the groundmass of the granodiorite. Quartz is a common mineral in the groundmass of the host rocks, and also in the ore-bearing veins. Based on mineralogical studies, seven vein types were distinguished in the biotitic alteration subzone, of which the first type listed in Table 1 is the most common ore-bearing vein. The ore assemblage dominated by pyrite and chalcopyrite, with minor bornite, is mostly disseminated (Fig. 6d).

4.2.2. Phyllic alteration

Phyllic alteration is restricted to drill cores, and also to the central regions of the surface exposures (Fig. 3b and c). Due to progressive destruction of silicate minerals except quartz, outcrops pervasively affected by sericite replacement are mostly white to whitish grey in color. The common rock-forming minerals are completely replaced by sericite and quartz in some samples, leaving no trace of the primary minerals, whereas the remnants of primary minerals, such as K-feldspar are observed in the partially altered samples. This zone is dominated by ubiquitous quartz, sericite, and pyrite, with lesser chalcopyrite (Fig. 6e). Sericite appears as inclusions within the partially altered K-feldspar phenocrysts, mixed with fine-grained matrix quartz, or as fine aggregates replacing coarse-grained sericite. The main sulfide minerals in the phyllic alteration are pyrite and lesser chalcopyrite, as disseminated and spongy aggregates, forming up to 10 vol% of the altered rocks. Quartz-sericite-pyrite ± chalcopyrite and pyrite veinlets are the most common vein types in this alteration zone, with quartz-sericite-pyrite veins surrounded by a halo of the phyllic assemblage (Table 1).

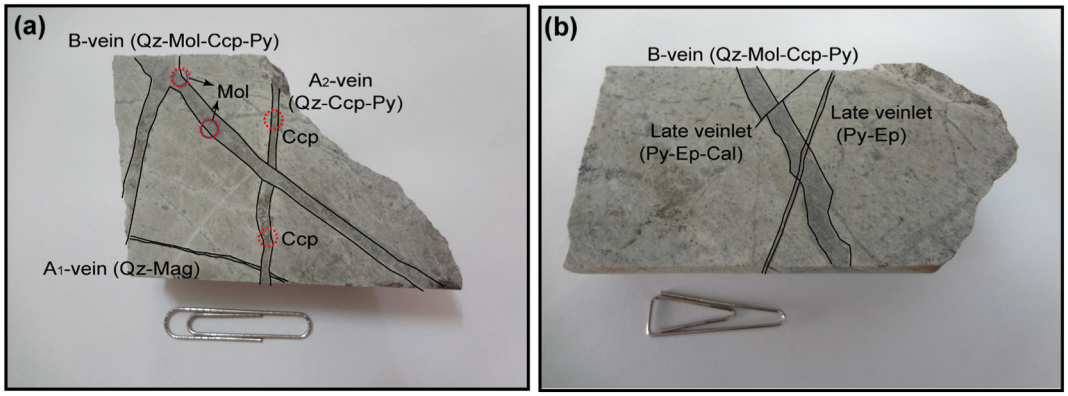

Fig. 5. Photographs of crosscutting relationships of the veins in hand specimens for the Zefreh porphyry Cu-Mo deposit. (a) The A_2-type vein cut by the B-type vein, but crosscut the A_1-type vein in the K-feldspar alteration. (b) The A_2-vein crosscut and offset by late veinlets in the biotitic alteration. Abbreviations as in Fig. 4.

Table 1
Summary of the petrographic observations of the alteration zones and vein types in the Zefreh porphyry C4u-Mo deposit. The most common ore-bearing veins are shown in bold type.

Alteration zone	Alteration minerals	Vein type	Width of vein (mm)	Sulfide assemblage	Style of sulfide mineralization
K-feldspar	Qz, Kfs, Bt ± (Mag, Chl, Ep)	**Qz-Py-Ccp-Mol ± Chl ± Ep**	3–4.5	Py + Ccp + Mol ± Cct ± Dg	Abundant: D and S
		Qz-Py-Ccp ± Chl	2–3		Not common: V and R
		Qz-Mag ± Ccp ± Chl	< 1		
		Sulfide-absent quartz veins	< 1		
Biotitic	Qz, Bt, Kfs ± (Mag, Pl)	**Qz-Py-Ccp ± Chl ± Ep ± Cal**	3.5–5	Py + Ccp ± Bn ± Dg	Abundant: D and S
		Qz-Py ± Bt ± Cal	1		Not common: V and R
		Qz-Bt-Mag-Kfs ± Ccp	< 2		
		Qz-Chl	1–2		
		Py	Very narrow (< 1)		
		Chl	Very narrow (< 1)		
		Sulfide-absent quartz veins	Very narrow (< 1; rarely 7.5)		
Phyllic	Qz, Ser, Py ± (Kfs, Ccp)	**Qz-Ser-Py ± Ccp**	2	Py ± Ccp	Abundant: D and S
		Py	Very narrow (< 1)		Not common: V
Argillic	Qz, Kln, Mnt, Gth, Lm ± (Chl, Ser, Py)	–	–	Py	Abundant: D
Propylitic	Qz, Chl, Ep ± (Kfs, Pl, Ser, Cal)	**Qz-Py-Ccp-Mol ± Chl ± Ep ± Ser ± Cal**	1–6 (rarely 8)	Py + Ccp + Mol ± Dg ± Bn ± Sp ± Gn	Abundant: D and S
		Qz-Py-Ccp ± Chl ± Ep	1–5 (rarely 8)		Not common: V and R
		Qz-Chl-Py ± Ep ± Cal	3.5		
		Qz-Chl-Ep ± Py	1		
		Qz-Ep-Py	Very narrow (< 1)		
		Ep-Cal-Py	Very narrow (< 1)		
		Chl-Ep-Py	Very narrow (< 1)		
		Chl	Very narrow (< 1)		
		Py	Very narrow (< 1)		
		Sulfide-absent quartz veins	Very narrow (< 1)		

Mineral abbreviations follow Whitney and Evans (2010). Bn = bornite, Bt = biotite, Cal = calcite, Ccp = chalcopyrite, Cct = chalcocite, Chl = chlorite, D = disseminated, Dg = digenite, Ep = epidote, Gn = galena, Gth = goethite, Kfs = K-feldspar, Kln = kaolinite, Lm = limonite, Mag = magnetite, Mnt = montmorillonite, Mol = molybdenite, Pl = plagioclase, Py = pyrite, Qz = quartz, R = replacement, S = stockwork, Ser = sericite, Sp = sphalerite, V = veinlet.

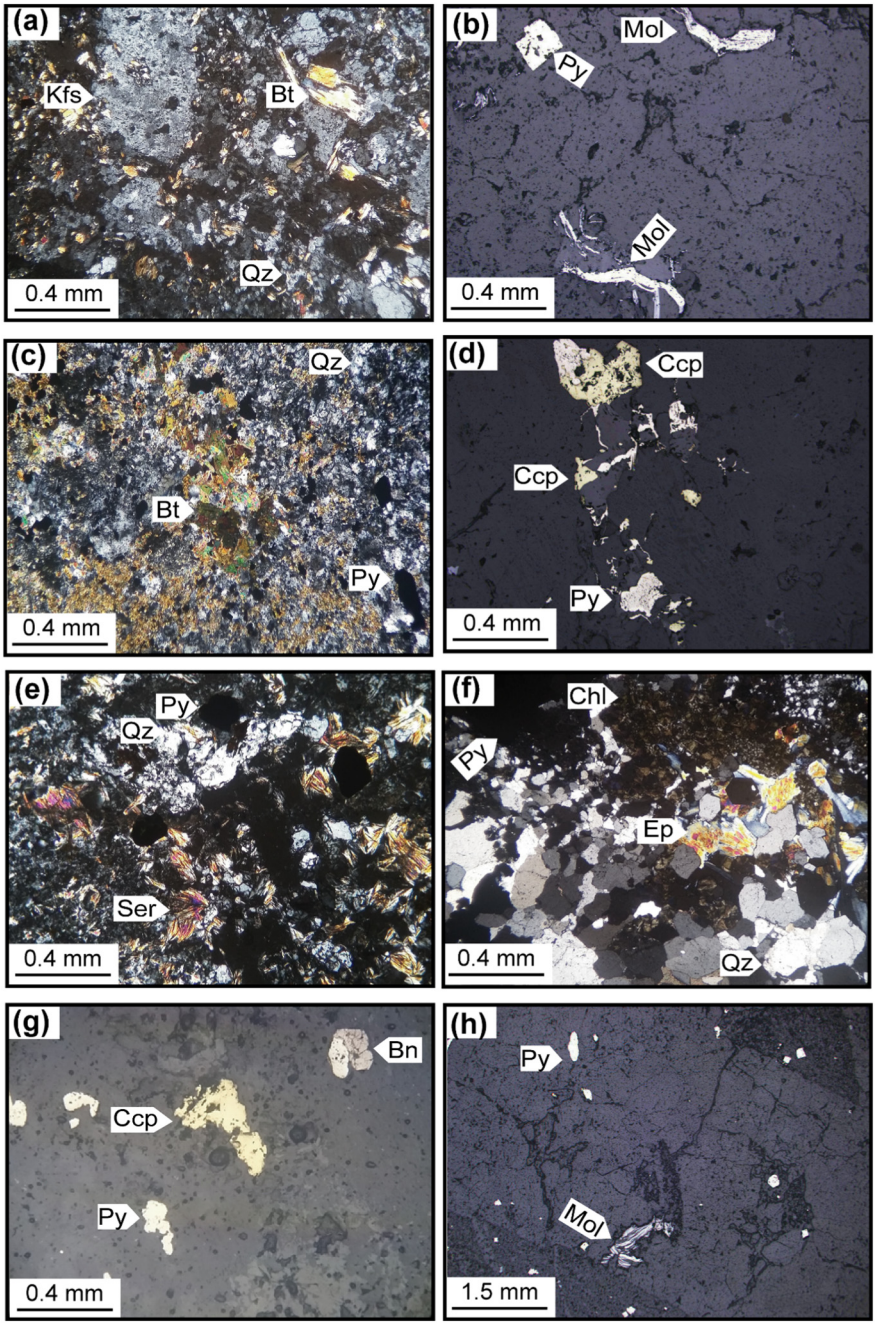

Fig. 6. Photomicrographs of different alteration types and the ore-bearing veins for the Zefreh porphyry Cu-Mo deposit. (a) K-feldspar alteration (XPL). (b) Molybdenite and pyrite in the quartz-dominated veins of the K-feldspar alteration (PPL). (c) Biotitic alteration (XPL). (d) Chalcopyrite and pyrite in the biotitic alteration (PPL). (e) Quartz, pyrite, and sericite in the phyllic alteration (XPL). (f) Propylitic alteration (XPL). (g) Chalcopyrite, pyrite, and bornite in the propylitic alteration (PPL). (h) Molybdenite and pyrite in the quartz-dominated veins of the propylitic alteration. Abbreviations as in Fig. 4.

4.2.3. Argillic alteration

Argillic alteration is found both in the surface exposures and in the shallowest parts of drill cores. It is characterized by quartz and clay minerals (e.g., kaolinite and montmorillonite), limonite, goethite, with lesser amounts of chlorite and sericite. This hydrothermal alteration is devoid of ore-bearing veins, and has only minor disseminated pyrite, confirming its formation during the latest stage of hydrothermal activity and mineralization.

4.2.4. Propylitic alteration

Propylitic alteration occurs both in the peripheral parts of the deposit in surface exposures and in the deeper parts of drill cores, adjacent to the potassic alteration zone. The common alteration minerals in the propylitic alteration are quartz, chlorite, and epidote, coupled with minor K-feldspar, plagioclase, sericite, and calcite (Fig. 6f). Epidote occurs as radial, bunched, or patchy replacements of plagioclase phenocrysts. Volumetrically, in the Zefreh deposit, the propylitic alteration zone and its veins and veinlets form almost the greater part of the alteration zones, compared to the other recognized hydrothermal alteration zones. Among ten types of veins identified in the propylitic alteration zone, the first two types listed in Table 1 are the most common ore-bearing veins (A_2 and B types). The chlorite, pyrite, and pyrite-epidote-calcite veins are late and barren, and commonly cut the early formed veins. Sulfides in the ore-bearing, quartz-dominated veins are pyrite, chalcopyrite, and molybdenite, with minor digenite and bornite (Fig. 6g and h).

4.3. Geochemistry

Whole-rock major and trace element analyses of 27 rocks (dacite, granodiorite, and granite) from the Zefreh area, along with important ratios of trace elements are presented in Table 1 in the Electronic Supplementary material. For geochemical interpretation and petrologic classification, major element oxides have been normalized to 100% on a volatile-free basis. SiO_2 contents in the granodioritic samples range from 60.7 to 64.5 wt% (average 62.3 wt%), for the dacitic samples 62.7–66.3 wt% (average 65.1 wt%), and for the granitic samples 62.7–65.5 wt% (average 64.6 wt%). Concentrations of Sr, Y, and Yb in the granodioritic samples are in the range of 251–355 ppm for Sr (average 287 ppm), 15–18 ppm for Y (average 17 ppm), and 1.6–2.2 ppm for Yb (average 2 ppm). Concentrations of these elements in the dacitic samples are 189–327 ppm for Sr (average 257 ppm), 20–46 ppm for Y (average 33 ppm), and 2.7–4.2 ppm for Yb (average 3.6 ppm), and in the granitic samples 234–567 ppm for Sr (average 336 ppm), 13–36 ppm for Y (average 24 ppm), and 1.4–3.5 ppm for Yb (average 2.5 ppm). $(La/Yb)_N$ ratios in the granodioritic, granitic, and dacitic samples are in the range of 3.6–5.6 (average 4.7), 2.3–4.3 (average 3.1), and 2–5.3 (average 3.4), respectively. Selected ratios in the Zefreh magmatic suite have 5–23 Sr/Y (average 11), 3–8 La/Yb (average 5), and 1.2–2 Dy/Yb (average 1.5). A comparison of the Zefreh magmatic suite with the ore-hosting (Kuh Panj) and non-productive (Jebal Barez) porphyry granitoids in the KCMA, the southeastern part of the UDMA, on the basis of some petrographic and geochemical features is presented in Table 2.

The bulk composition of the Zefreh least-altered rocks plots in the sub-alkaline field of the total alkali versus silica diagram (Le Maitre et al., 2002), and ranges from diorite to granodiorite in composition (Fig. 7a). On the K_2O versus SiO_2 diagram (Peccerillo and Taylor, 1976), the Zefreh rocks falls within the low- to medium-K calc-alkaline series, distinctly lower in K_2O than the adakites (Fig. 7b). The Zefreh rocks (granite, granodiorite, and dacite) are enriched in Th, U, and some large ion lithophile elements (LILE; e.g., Rb and Pb), but depleted in Ti, Nb, Ta, Ba, Sr, and P (Fig. 8a–c). Compared with the granodioritic and granitic samples, however, the dacitic samples exhibit more enrichment in Th, U, and Pb. The chondrite-normalized REE patterns reveal enrichments of LREE relative to MREE, generally flat patterns from MREE to HREE, and negative Eu anomalies in the most differentiated rocks (Eu/Eu* = 0.5–1.1, average 0.8; Fig. 9a–c). The granodioritic and granitic samples are characterized by no negative to slightly positive Eu anomalies, moderate contents of Y and Yb, and moderate Sr/Y ratios. In contrast, the dacitic samples are characterized by strong negative Eu anomalies, low to moderate Sr contents, and low to moderate Sr/Y ratios.

5. Discussion

5.1. Geochemical affinity of the granitoids

The more evolved members of the Zefreh magmatic suite are similar in chemical composition to the experimental melts of low- to medium-K amphibolite (Fig. 7b), but a simple source model for the whole suite cannot explain the increasingly low-K character of the most evolved samples, may be related to fractionation. As shown in Fig. 10a and b, they also exhibit low FeOt/MgO at a given SiO_2 content, suggestive of calc-alkaline differentiation. Magnetic susceptibility of the Zafarghand granitoid rocks, < 30 km NE of the Zefreh area, ranges from 9885 μSI to 38,120 μSI, corresponding to their provenance from the magnetite-series granitic rocks (Gavanji, 2010). The Zefreh fractionated granitoids are also classified as magnetite-series in the Fe_2O_3/FeO vs. SiO_2 diagram of Ishihara (1977). Moreover, these indicate that the porphyry-style mineralization at Zefreh was genetically related to oxidized I-type, intermediate-to-acidic (dacite, granodiorite, and granite) subvolcanic magmas, in which sulfur is present in the oxidized form of SO_4^{2-}

Table 2
Petrographic and geochemical comparison between the Zefreh granitoids and the representative granitoid rocks in the KCMA (Kuh Panj-type and Jebal Barez-type).

Magmatic suite	Rock type	Main texture	Magmatic series	Ore minerals	Alteration zones	Tectonic setting	Sr (ppm)	Y (ppm)	Sr/Y	La/Yb	Eu/Eu*
Kuh Panj-type (n = 15)	Major: Dr-Qdr and Qdr Minor: Gd and Qmz[A]	Porphyry and fine-porphyry[A]	Adakite-like[A]	Major: Ccp + Py Minor: Mol ± Bn ± Mag[B]	Potassic ± transitional potassic-phyllic + phyllic + argillic + propylitic[B]	Syn- to post-collisional[A]	406–1015 (759)[A]	5–18 (10.7)[A]	33.8–112.8 (76.9)[A]	19.1–53.1 (29.6)[A]	1–1.3 (1.1)[A]
Jebal Barez-type (n = 22)	Major: Dr-Qdr and Qdr Minor: Qmz[A]	Equigranular[A]	Normal calc-alkaline[A]	Minor: Ccp ± Py[B]	Phyllic + propylitic ± argillic[B]	Pre-collisional[A]	184–576 (339)[A]	12–29 (20.4)[A]	6.6–33.9 (18.1)[A]	2.5–14.7 (6.9)[A]	0.6–1 (0.9)[A]
Zefreh area (n = 27)	Major: Gd, G, and D[C]	Porphyry[C]	Normal calc-alkaline[C]	Major: Py Minor: Ccp + Mol[C]	K-feldspar + biotitic + phyllic + argillic + propylitic[C]	Pre-collisional[C]	189–567 (279)[C]	12.6–45.6 (28.5)[C]	4.7–23.2 (11)[C]	2.8–7.7 (5)[C]	0.5–1.1 (0.8)[C]

Abbreviations: Dr-Qdr = diorite-quartz diorite, Qdr = quartz diorite, Qmz = quartz monzonite, Gd = granodiorite, G = granite, D = dacite. Mineral abbreviations as in Table 1.
Kuh Panj-type granitoids: Sar-Cheshmeh, Meiduk, Darreh Zar, Abdar, Iju, Kader, Chah Firuzeh, Saridume, and Parkam[A].
Jebal Barez-type granitoids: Reagan, Dar Alu, Archandor, and Bagh Khoshk[A].
(A) Shafiei et al. (2009). (B) Asadi et al. (2014). (C) This study.

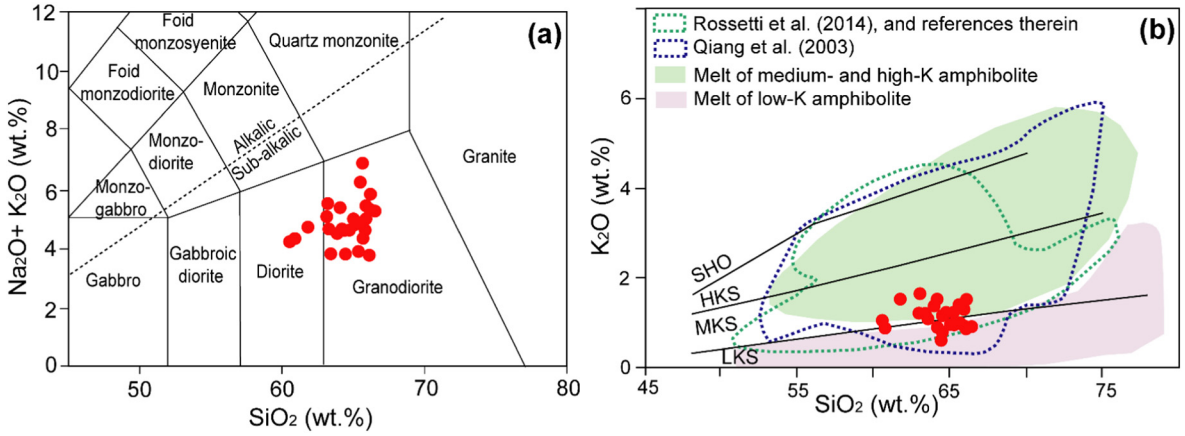

Fig. 7. Plot of the Zefreh rocks in (a) total alkali versus silica diagram ($Na_2O + K_2O$ versus SiO_2; Le Maitre et al., 2002) and (b) the K_2O versus SiO_2 diagram (Peccerillo and Taylor, 1976). The alkalic/sub-alkalic boundary of Irvine and Baragar (1971) is shown. The fields of adakites are from Qiang et al. (2003) and Rossetti et al. (2014), and references therein, and melts from Lu et al. (2013). Abbreviations: SHO = shoshonite series, HKS = high-K calc-alkaline series, MKS = medium-K calc-alkaline series, LKS = low-K calc-alkaline series.

(Mungall, 2002; Sillitoe, 2010). Oxidizing conditions prevent the separation of Cu-sulfide melts from such magmas, and may lead to the concentration of chalcophile elements in the evolved magmas. Deposition of chalcophile elements, such as Cu and Mo was most probably be controlled by the behavior of reduced sulfur, which requires sulfate reduction in the oxidized magmas (Mungall, 2002). The resultant hydrosulfide complexes would tend to scavenge these elements from the primary magma into aqueous mineralizing fluids (Mungall, 2002).

On the Al_2O_3 versus TiO_2 diagram (Müller et al., 1992), the Zefreh granitoids similar to the Kerman granitoid rocks and the Dalli intrusions plot in the field of arc-related magmas (Fig. 11a). As shown in Fig. 11b, the Zefreh rocks mainly plot in the fields of mantle fractionation and pre-collisional environment. The Dalli intrusions also plot in a pre- to post-collisional tectonic setting in the R1 (4Si-11(Na + K)-2(Fe + Ti)) vs. R2 (6Ca + 2 Mg + Al) diagram of Batchelor and Bowden (1985). Whereas, the Kerman ore-hosting granitoids mainly plot in a post-collisional tectonic setting, which is consistent with evolution of the magmatic arc system and arc crustal thickening during the Neo-Tethyan Ocean closure and the Alpine-Himalayan collision in central Iran (Shafiei et al., 2009). Furthermore, the Zefreh rocks occur in primitive

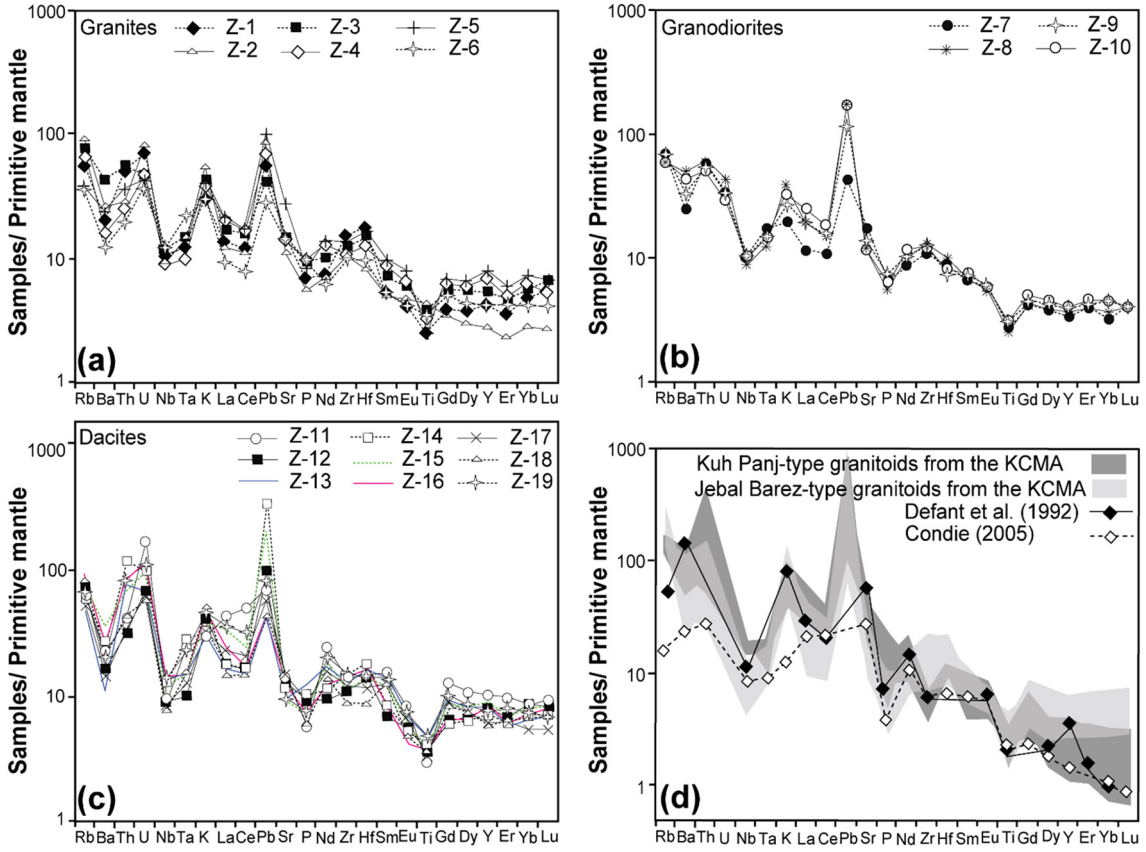

Fig. 8. Primitive mantle-normalized multi-element spider diagrams for the granitic (a), granodioritic (b), and dacitic (c) samples of the Zefreh area, and adakites and the representative granitoid rocks in the KCMA (Kuh Panj-type and Jebal Barez-type) (d). Values of the primitive mantle are from Sun and McDonough (1989). Data: adakites (Defant et al., 1992; Condie, 2005), Kuh Panj-type and Jebal Barez-type porphyry granitoids (Shafiei et al., 2009).

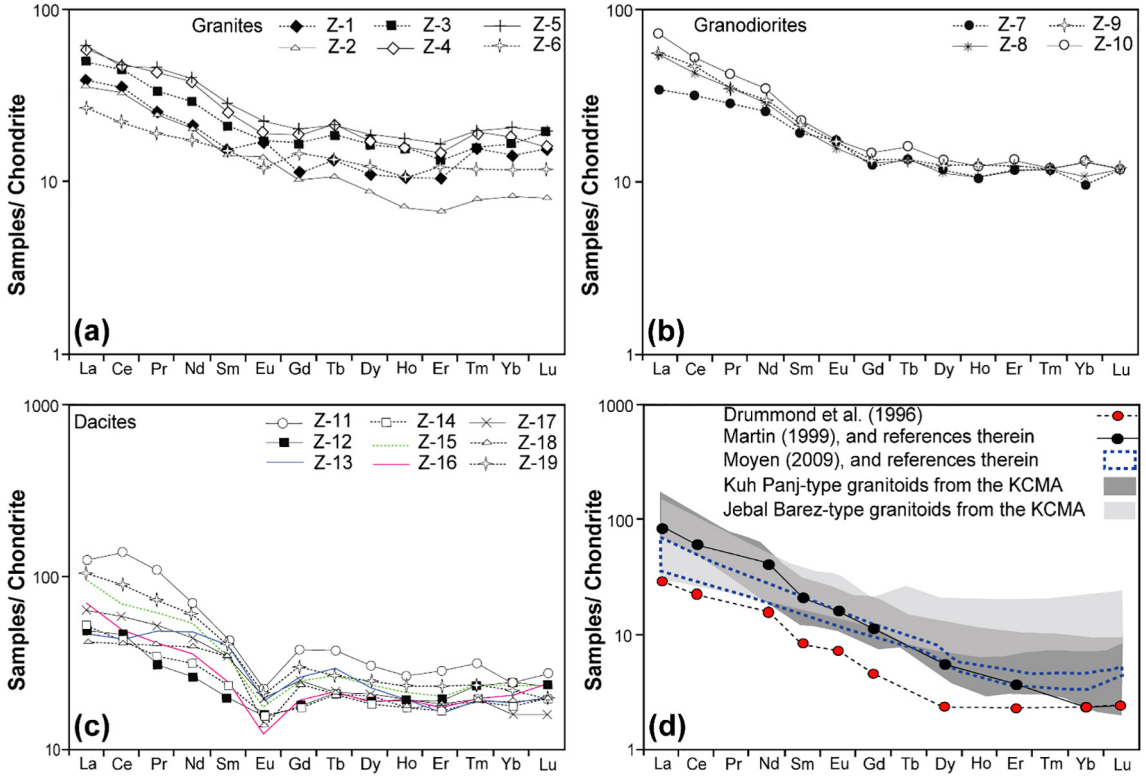

Fig. 9. Chondrite-normalized REE patterns for the granitic (a), granodioritic (b), and dacitic (c) samples of the Zefreh area, and adakites and the representative granitoid rocks in the KCMA (Kuh Panj-type and Jebal Barez-type) (d). Values of the Chondrite are from Sun and McDonough (1989). Data: adakites (Drummond et al., 1996; Martin, 1999, and references therein; Moyen, 2009, and references therein), Kuh Panj-type and Jebal Barez-type porphyry granitoids (Shafiei et al., 2009).

arc maturity, before the arc continental collision relative to the Dalli intrusions and the Kuh Panj-type porphyry granitoids formed in a continental collision setting (Fig. 11c).

5.2. Source indicators

For the Zefreh granitoids, enrichments in some LILE (e.g., Rb and Pb), and depletions in Nb and Ta in the primitive mantle-normalized multi-element diagrams (Fig. 8a–c), and enrichments of LREE relative to HREE in the chondrite-normalized REE patterns (Fig. 9a–c) are characteristic of the subduction-related arc magmas (Sun and McDonough, 1989). Enrichments in Rb, Th, U, and Pb, and negative Nb, Ta, Ba, P, Sr, and Ti anomalies in the spider diagrams (Fig. 8a–c) indicate that the Zefreh rocks are genetically fractionated granitoids. According to Fig. 12a, the Zefreh granitoid rocks closely resemble the barren (normal calc-alkaline) Jebal Barez porphyry granitoids in the KCMA, and the Ardestan and Zafarghand granitoids in the SYMA, but differ from the ore-hosting (adakite-like) Kuh Panj porphyry granitoids in the KCMA and the Dalli intrusions in the SYMA. Although showing some geochemical characteristics resembling adakites (e.g., average content of major oxides, such as SiO_2, Al_2O_3, MgO, Na_2O, and K_2O, and trace elements, such as Rb similar to adakites; Table 3; cf. Richards and Kerrich, 2007), the Zefreh rocks show a normal calc-alkaline signature in geochemical diagrams (Fig. 12a and b) and other geochemical characteristics. These characteristics include low to moderate Sr contents, moderate to high contents of Y and Yb, low to moderate Sr/Y

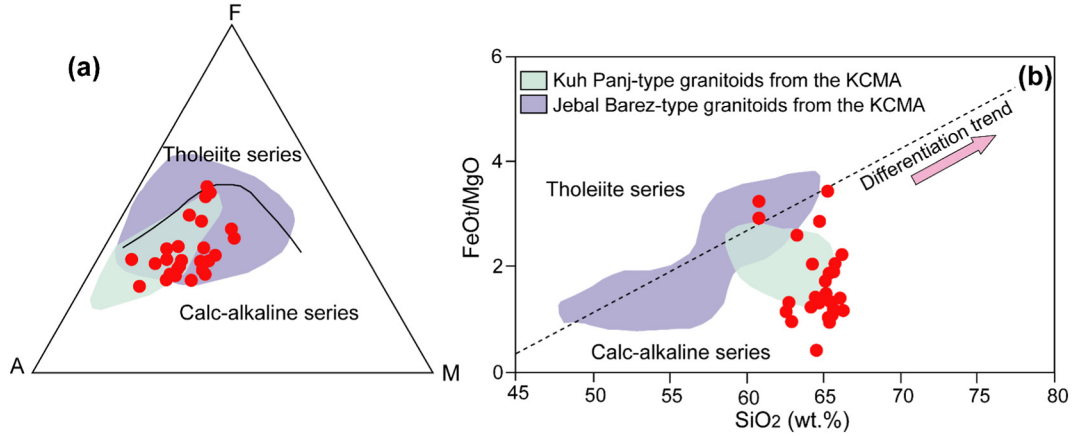

Fig. 10. The Zefreh granitoid rocks shown in (a) (Na_2O + K_2O)-(FeO + Fe_2O_3)-MgO diagram (AFM; Irvine and Baragar, 1971) and (b) FeOt/MgO versus SiO_2 diagram (Miyashiro, 1974). Data for the Kuh Panj-type and Jebal Barez-type porphyry granitoids from the KCMA are from Shafiei et al. (2009).

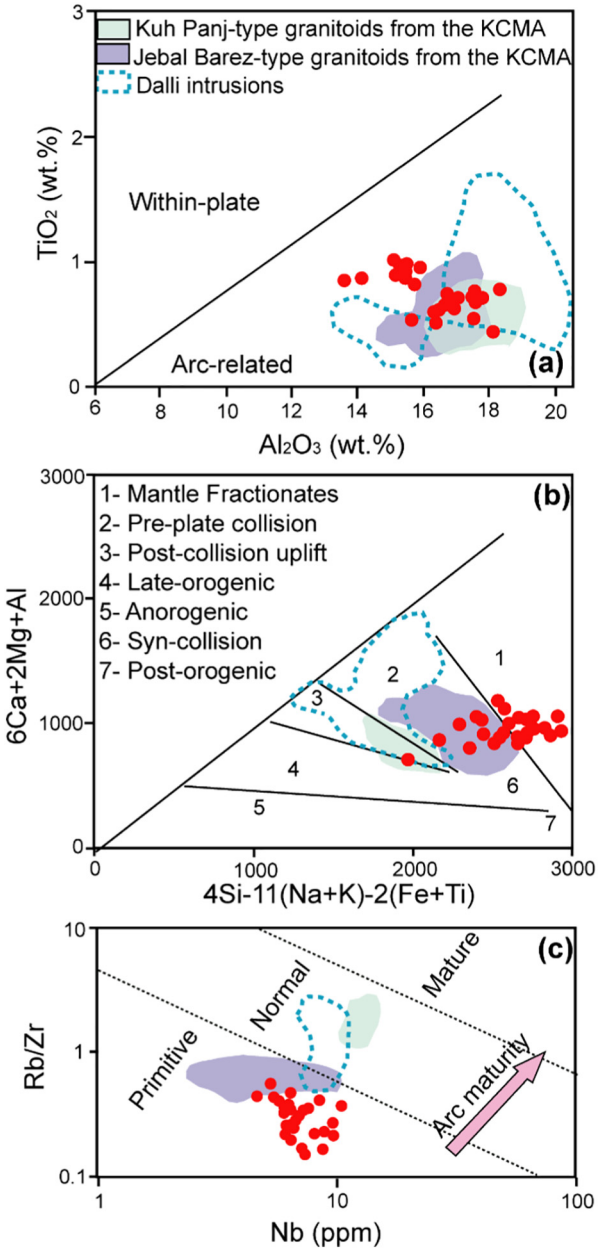

Fig. 11. Plot of the Zefreh granitoids in (a) Al_2O_3 vs. TiO_2 diagram (Müller et al., 1992), (b) R1 (4Si-11(Na + K)-2(Fe + Ti)) vs. R2 (6Ca + 2 Mg + Al) diagram (Batchelor and Bowden, 1985), and (c) Rb/Zr vs. Nb diagram (Brown et al., 1984). Data: Kuh Panj-type and Jebal Barez-type porphyry granitoids from the KCMA (Shafiei et al., 2009), Dalli intrusions (Zarasvandi et al., 2015).

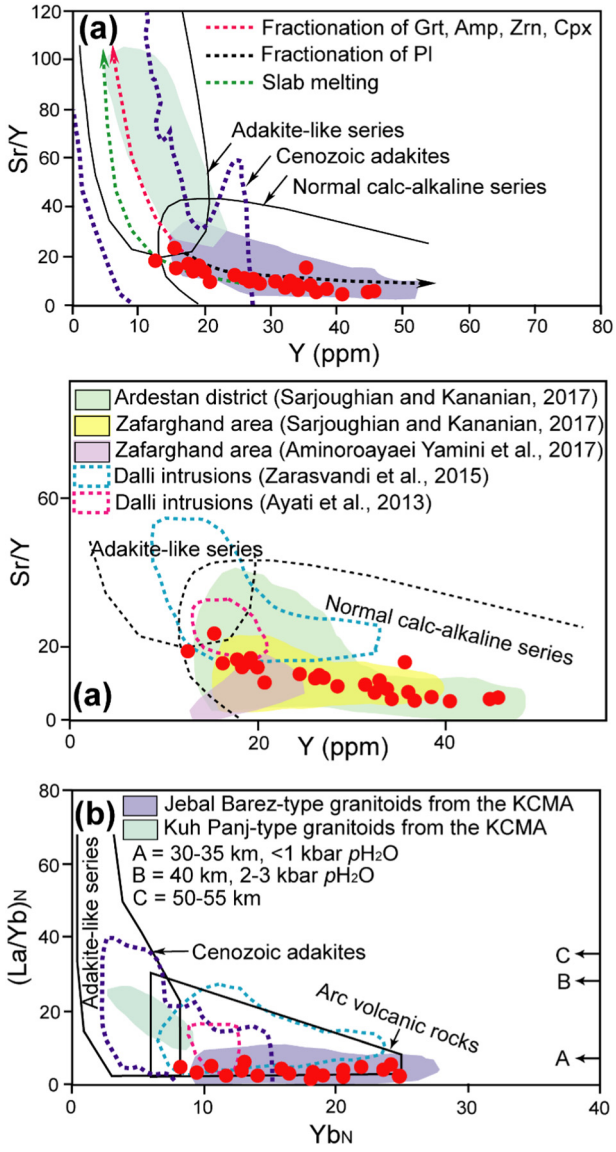

Fig. 12. Representative samples of the Zefreh area in (a) Sr/Y-Y diagram and (b) $(La/Yb)_N$-$(Yb)_N$ diagram (Defant and Drummond, 1990). The fields of the Cenozoic adakites are from Rossetti et al. (2014), and references therein. Data: Kuh Panj-type and Jebal Barez-type porphyry granitoids from the KCMA (Shafiei et al., 2009), Dalli intrusions (Ayati et al., 2013; Zarasvandi et al., 2015), intrusive rocks in the Zafarghand area (Aminoroayaei Yamini et al., 2017; Sarjoughian and Kananian, 2017), intrusive rocks in the Ardestan district (Sarjoughian and Kananian, 2017). Abbreviations as in Fig. 4.

ratios, and low La/Yb ratios in the studied samples. Hence, it can be inferred that the Zefreh magmatic suite did not originate from a hydrous adakitic magma in the lower crust. Considering low to moderate Sr/Y ratios and low La/Yb ratios of the rocks, and immature arc (pre-collisional tectonic setting), the Zefreh deposit is likely to be a small, sub-economic PCDs than a high-grade and economic PCDs.

Moderately fractionated REE patterns (or moderate $(La/Yb)_N$ ratios) and concave-upward shapes from MREE to HREE in the chondrite-normalized REE patterns reflect fractionation of hornblende (Richards and Kerrich, 2007; Shafiei et al., 2009). The overall REE patterns of the Zefreh evolved samples are characterized by enrichments of LREE relative to MREE and HREE, and flat to listric-shaped MREE-HREE patterns (Fig. 9a–c). Compared with the dacitic samples, however, the granodioritic samples are characterized by more high $(La/Yb)_N$ ratios and no negative to slightly positive Eu anomalies, which are consistent with moderate contents of Sr, Y, and Yb, and moderate Sr/Y ratios. These geochemical features suggest intermediate crustal depth and moderate magmatic water content of the subduction-related arc magma (Davidson et al., 2007). Patterns from the ore-hosting (adakite-like) Kuh Panj porphyry granitoids in the KCMA and adakites are almost the same (Fig. 9d). The slope of LREE enrichments in the most differentiated rocks at Zefreh is lower than the Kerman ore-hosting (Kuh Panj) granitoids, which is likely attributed to higher degrees of mantle partial melting (Almeida et al., 2007). In the KCMA, the productive adakite-like (Kuh Panj) granitoids are characterized by overall steeper REE profiles, due to the more LREE-enriched and HREE-depleted signatures (or high La/Sm and Sm/Yb ratios) than the non-productive (Jebal Barez) granitoids (Fig. 9d). Furthermore, the syn- to post-collisional Kuh Panj-type granitoids, exhibit slightly less positive Eu

Table 3
Comparison of geochemical features of the Zefreh rocks and adakites (Richards and Kerrich, 2007).

	SiO_2 (wt%)	Al_2O_3 (wt %)	MgO (wt%)	Na_2O (wt%)	K_2O (wt %)	Rb (ppm)	Sr (ppm)	Y (ppm)	Yb (ppm)	Ni (ppm)	Na_2O/K_2O	Sr/Y	La/Yb
Adakites	≥56	≥15	< 3	≥3.5	≤3	≤65	≥400	≤18	≤1.9	≥20	0.42	≥20	≥20
Zefreh magmatic suite	60.7–66.3 (64.6)	13.4–18.2 (16.3)	1.1–4 (2.5)	2.4–5.5 (3.7)	0.6–1.6 (1.1)	23–49 (41)	189–567 (279)	12.6–45.6 (28.5)	1.4–4.2 (2.9)	3–15 (6)	1.9–5.7 (3.5)	4.7–23.2 (11)	2.8–7.7 (5)

anomalies than the pre-collisional Jebal Barez-type granitoids (Fig. 9d and Table 2). These positive Eu anomalies are consistent with residual amphibole and/or garnet in the lower crustal source rocks, and hydrous and highly oxidized nature of the adakitic magmas (Shafiei et al., 2009; Richards et al., 2012). Whereas, the normal calc-alkaline rocks that display right dipping REE patterns, undepleted HREE, and negative Eu anomalies are rarely associated with large, productive porphyry deposits (Qiang et al., 2003). In this regard, it is suggested that the Zefreh deposit is likely to be a small, sub-economic porphyry Cu-Mo deposit.

The REE variation diagrams exhibit distinct negative anomalies of Eu for the dacitic rocks at Zefreh (Fig. 9c). The granitic and granodioritic samples with (Eu/Eu*) close to unity or slightly higher, correlate with higher Sr/Y, suggesting plagioclase accumulation and/or amphibole fractionation. Correlation between Y and SiO_2 in the Zefreh granitoid rocks argues against fractionation of garnet from the primitive magma (Fig. 13a; Richards and Kerrich, 2007). On the MgO-SiO_2 diagram of Rapp et al. (1999), the majority of the Zefreh samples are far from the fields of adakites and the Kuh Panj-type porphyry granitoids (Fig. 13b). On the MgO vs. La/Yb diagram, the Zefreh data also are far from the fields of adakites, the ore-hosting (adakite-like) Kuh Panj porphyry granitoids in the KCMA, and the Dalli granitoids in the SYMA (Fig. 13c). Low La/Yb ratios in the Zefreh granitoid rocks rule out considerable amounts of fractionated amphibole from a hydrous magma. The probable absence of hydrous and oxidized adakitic magmas in the lower crust likely results in the formation of some small, low-grade PCDs in the SYMA (e.g., the Zafarghand and Zefreh deposits), and also in the KCMA (e.g., the Jebal Barez-type deposits). Considering La/Yb as a crustal thickness proxy in intermediate calc-alkaline rocks (Profeta et al., 2015), arc crustal thickness in the Zefreh area was probably < 40 km at the time of emplacement of normal calc-alkaline granitoids (Fig. 13c). According to Fig. 14, the Zefreh samples plot close to the field of partial melting of an amphibolite source, and are almost distinct from the Kerman ore-hosting (Kuh Panj) granitoids generated by partial melting of the garnet-bearing lower-crustal amphibolites in a thickened arc crust (40–50 km; Shafiei et al., 2009) and adakites. Based on experimental partitioning data of Foley et al. (2002), generation of the Zefreh magmatic suite is consistent with < 10% batch melting of a garnet-free amphibolite source at moderate pressure (0.8 GPa; Fig. 14). This result is consistent with low to moderate Nb/Ta ratios and obvious negative anomalies of Nb in the studied rocks (Figs. 8a-c). Nb/Ta values of the Zefreh granitoid rocks and the Kerman adakite-like (Kuh Panj-type) granitoids range from 6.4–17.2 (average 12) to 12.5–23.5 (average 17.9), respectively. This significant difference in the Nb/Ta ratio likely implies a substantial gradient in crustal thickness between the central and southeastern parts of the UDMA, the SYMA and KCMA, respectively. Geochemical data indicate that the Zefreh granitoids formed in a pre-collisional tectonic setting, whereas the ore-hosting (Kuh Panj) porphyry granitoids in the KCMA formed in a syn- to post-collisional tectonic setting, and situated in an orogenic and exhumed arc crust (40–50 km; Shafiei et al., 2009). Arc crustal thickness in the Zefreh area was not possibly thick enough to fractionate amphibole considerably in the lower crust assemblage crystallizing from an oxidized magma, probably caused sub-economic potential of the Zefreh porphyry Cu-Mo deposit.

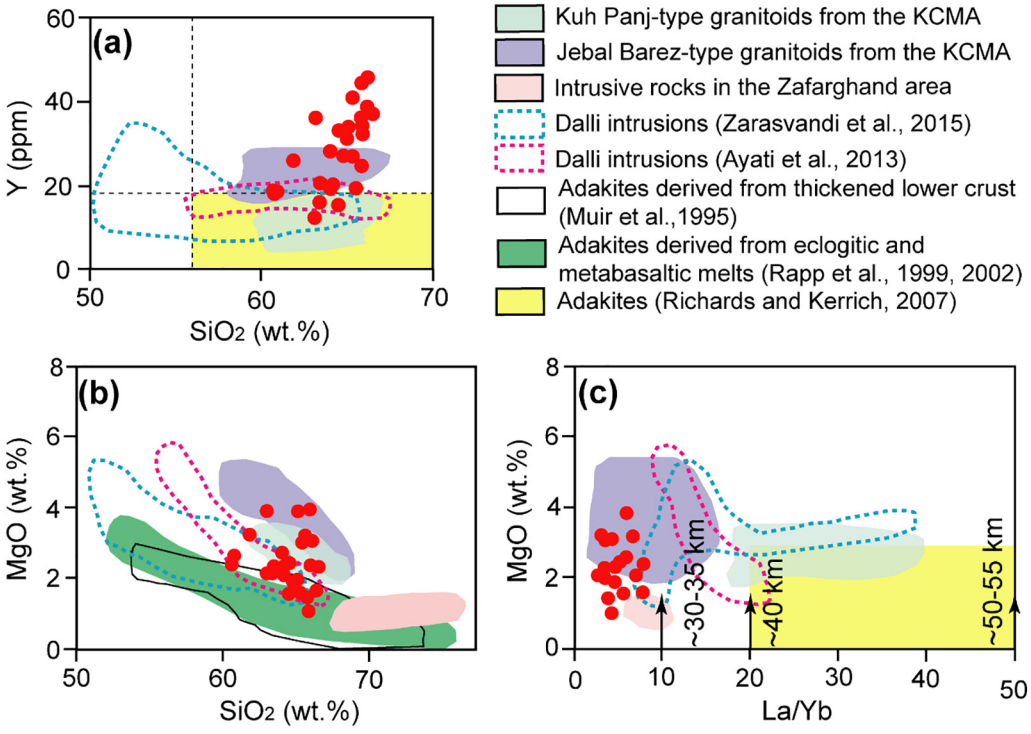

Fig. 13. (a) Plot of the Zefreh samples in Y-SiO_2 diagram (Richards and Kerrich, 2007) argues against fractionation of garnet from the primitive magma. Comparison of the Zefreh rocks with adakites and the representative granitoid rocks in the SYMA (Dalli and Zafarghand) and the KCMA (Kuh Panj-type and Jebal Barez-type) in (b) SiO_2-MgO diagram (Rapp et al., 1999) and (c) La/Yb-MgO diagram. Average crustal thickness, on the basis of La/Yb ratio is from Ahmadian et al. (2009). The fields of adakites are from Muir et al. (1995), Rapp et al. (1999, 2002), and Richards and Kerrich (2007). Data: Kuh Panj-type and Jebal Barez-type porphyry granitoids (Shafiei et al., 2009), Dalli intrusions (Ayati et al., 2013; Zarasvandi et al., 2015), Zafarghand intrusions (Aminoroayaei Yamini et al., 2017).

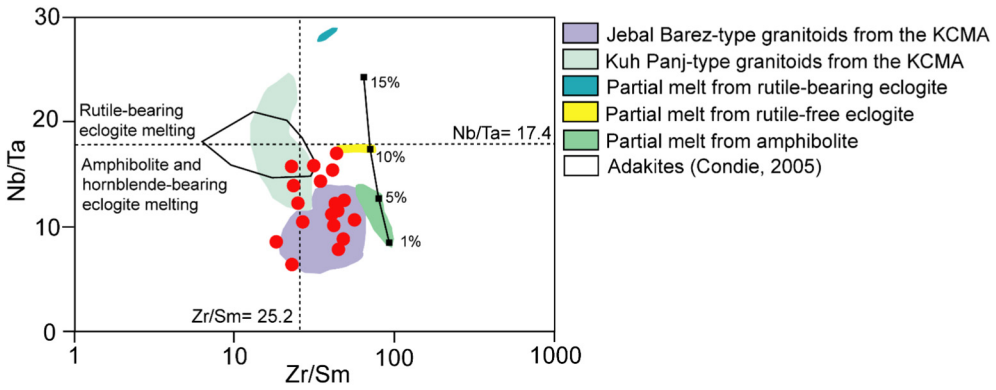

Fig. 14. Nb/Ta versus Zr/Sm diagram (Foley et al., 2002; Yin et al., 2017) for the Zefreh magmatic suite. Primitive mantle composition (Nb/Ta = 17.4 and Zr/Sm = 25.2) is from Sun and McDonough (1989). The field of adakites is from Condie (2005) and melts from Yin et al. (2017). Data: Kuh Panj-type and Jebal Barez-type porphyry granitoids from the KCMA (Shafiei et al., 2009).

5.3. Petrogenesis and economic potential of the deposit

A comprehensive petrogenetic model for the normal calc-alkaline magmatic suite at Zefreh should be constructed, on the basis of petrographic and geochemical studies, with isotopic data. Taking into account the close genetic relationship between the Cenozoic hydrous and oxidized granitoids and porphyry-style Cu mineralization in the UDMA, we provisionally rely on geodynamic evolution of volcanism and magmatism in the SYMA, and also on the U-Pb ages of zircon from intrusive rocks in the Ardestan district, especially in the Zafarghand area. There are some similarities between the Zefreh and Zafarghand mineralized systems, including geochemical characteristics of intrusive rocks (Fig. 12a; normal calc-alkaline signature), types of alteration (potassic, phyllic, argillic, and propylitic alteration zones), tectonic setting (pre-collisional environment), crustal thicknesses at the time of emplacement of the granitoids (< 40 km; Fig. 13c), and copper grade in ore reserves (< 0.4%). The Cenozoic volcanism and plutonism in the Ardestan district, constrained by the U-Pb dating on zircon from intrusive rocks, are divided temporally into three main magmatic episodes: Early-Late Eocene, Late Oligocene, and Early Miocene (Sarjoughian and Kananian, 2017). The emplacement age of the Zafarghand calc-alkaline granodiorite is attributed to the Late Oligocene (24.6 ± 1.0 Ma; Sarjoughian and Kananian, 2017), likely earlier than the Late Cenozoic continental closure and final collision event. The emplacement of intrusive rocks in the Ardestan district is attributed to evolution of the magmatic arc system from a subduction-related setting to a post-collisional setting over the time (Sarjoughian and Kananian, 2017). Chiu et al. (2013) believed that the onset of post-collisional magmatism (Late Miocene, 11 Ma) is coincident with the emplacement of the potassic to ultrapotassic rocks (absarokite or plagioleucitite), that outcrop in northwestern Iran (Saray, the east of Urumieh lake), Lesser Caucasus, and eastern Anatolia (NE Turkey). Progressive enrichment of the granitoids in Sr, with depletion in Y and HREE are not recorded in the Ardestan district, as a result of change in signature of granitoids from the normal calc-alkaline to the adakitic magmas over the time. Although this change in signature has been described in the southeastern part of the UDMA of Iran (or KCMA), which is attributed to transpressive crustal shortening and thickening during the Neo-Tethyan Ocean closure, and the Alpine-Himalayan collision from the Paleogene to the Neogene (Shafiei et al., 2009; Asadi et al., 2014).

Omrani et al. (2008) concluded that occurrence of the Neogene adakites in the SYMA represents a response to slab break-off and regional-scale thermal re-equilibration in a post-collisional tectonic setting. Other authors, though, attributed the Late Oligocene-to-Early Miocene adakitic volcanic successions in the central part of the SYMA to an asthenospheric upwelling associated with a slab roll-back (Yeganehfar et al., 2013). The concurrent Oligocene-Miocene volcanism and the Miocene adakitic rocks in the northern and central parts of the SYMA are thought to be also related to an asthenospheric mantle upwelling, coupled with a slab roll-back (Ghorbani et al., 2014). Generally, upwelling of fertile asthenosphere provides increasing temperature, together with melting of the sub-continental lithosphere mantle and/or mafic lower crust, favoring oxidized magmas that have potential to form large PCDs (Aghazadeh et al., 2015, and references therein). Generation of the Zefreh magmatic suite is not consistent with the aforementioned petrogenetic models, due to the normal calc-alkaline signature of the granitoids. Utilizing geochemical characteristics, with U-Pb and Sr-Nd isotopic data of the Zafarghand (normal calc-alkaline) granitoids, Sarjoughian et al. (2018) suggested that these granitoids formed through interaction between lower-crustal amphibolites and metabasalts, and mafic lower/middle-crustal rocks, together with fractional crystallization and crustal assimilation processes. The Zefreh granitoids also have a normal calc-alkaline character, which likely formed in a pre-collisional tectonic setting, prior to collision of the Arabian plate and the Central Iranian segment. Thus, available magmatic sources would have included the subducted oceanic slab, the mantle wedge metasomatized by slab fluids, and the mafic lower-crustal rocks. Partial melting of subducted oceanic slab is geochemically characterized by low Y and Yb contents, and high La/Yb and Sr/Y ratios, which are indicative of amphibole and/or garnet in the residual source. Therefore, it is unlikely that the Zefreh magmatic suite has been derived by melting of subducted oceanic slab, on the basis of geochemical characteristics of the granitoids (e.g., moderate to high contents of Y and Yb, low to moderate Sr/Y ratios, and low La/Yb ratios). No negative to slightly positive Eu anomalies in some differentiated rocks of the Zefreh area (e.g., granodioritic and granitic rocks) indicate plagioclase accumulation and/or amphibole fractionation. Partial melting of a garnet-free amphibolite source can explain moderate Sr/Y ratios of the granodioritic and some granitic samples, whereas peridotite melting and subsequent fractional crystallization of plagioclase can explain low to moderate Sr/Y ratios of the dacitic samples. In addition, negative Eu anomalies would develop with magma differentiation, because of fractional crystallization of early K-feldspar and/or plagioclase (Henderson, 1984), as seen in the dacitic samples. Therefore, it is suggested that some portions of the mantle-derived basaltic melts were emplaced at or near the mantle-crust boundary, forming mafic lower-crustal rocks. Such gabbroic/basaltic lower-crustal rocks metasomatized by the slab fluids would be transformed partially to amphibolite (e.g., Kay and Mahlburg-Kay, 1991). Such underplated lower-crustal amphibolite could be similar in geochemical and isotopic composition to calc-alkaline lavas that reach the surface (Borg and Clynne, 1998). Subsequent partial melting of these garnet-free lower-crustal amphibolites, together with fractional crystallization and crustal assimilation processes may thus be the main source of the Zefreh granitoids. Amphibole breakdown (or dehydration) in response to heating by continuing magmatic flux would release moderate quantities of water, and potentially increase oxygen fugacity (e.g., Davidson et al., 2007). Geochemical data suggest that arc crustal thickness was probably < 40 km at the time of emplacement of the granitoids at Zefreh. Furthermore, in the KCMA, arc crustal thickness in the Late Eocene was

30–35 km at the time of emplacement of the Jebal Barez-type granitoids, while, in the Middle to Late Miocene, it was 40–50 km at the time of emplacement of the adakite-like Kuh Panj granitoids (Shafiei et al., 2009). Qiang et al. (2003) proposed that only a small volume of magmatic fluids would tend to be released from a 40-km-thick basaltic crust, a factor commonly thought to be related to sub-economic, low-grade PCDs. On the basis of geochemical data, it is suggested that the Zefreh deposit is likely a small, sub-economic porphyry Cu-Mo deposit.

In the Zefreh area, breakdown of hydrous minerals would not proceed to a sufficient extent to drive major oxidation, and to concentrate sulfide phases. Without entrainment of sulfide droplets in the silicate melt, the volume of chalcophile elements prerequisite for the formation of economic-grade ore-hosting porphyry systems would not occur (Mungall, 2002). The lack of chalcopyrite and magnetite, and the absence of anhydrite in the microscopic sections of the potassic alteration at Zefreh indicate low sulfur concentrations and low oxygen fugacity. Lu et al. (2015) suggested that fluid-absent melting of amphibolite in the lower crust cannot produce high water melts. Another aspect of the ore-formation process was the possible occurrence of common volcanic eruptions from the top of the system (e.g., Ghasemi and Talbot, 2006; Shafiei et al., 2009; Asadi et al., 2014). The sulfur outgassing generally accompanies widespread volcanic activities in extensional or transtensional environments.

6. Conclusions

The Zefreh rocks range from diorite to granodiorite in composition. They exhibit a normal calc-alkaline signature of subduction-related arc magmas, rather than the hydrous and oxidized adakitic magmas thought to be commonly related to high-grade, economic porphyyr copper systems. The Zefreh granitoids are enriched in Th, U, Rb, Pb, and LREE, but depleted in Ti, Nb, Ta, Sr, Ba, and P. We propose that the crustal thickness in the Zefreh area was not probably sufficient to support lower crustal amphibole fractionation considerably from a hydrous magma, which is consistent with low to moderate Sr/Y ratios (5–23), low La/Yb ratios (3–8), and negative to slightly positive Eu anomalies (0.5–1.1; average 0.8). Melting of garnet-free lower-crustal amphibolites, together with fractional crystallization and crustal assimilation processes may be the main source of granitoids at Zefreh. Taking into account the intimate relationship between the hydrous and oxidized adakitic magmas and fertile metallogenic environment, as well as orogenic arc crust evolution for porphyry deposits in the UDMA, it is suggested that the Zefreh granitoids formed in a pre-collisional tectonic setting do not have potential to generate a high-grade, economic porphyry Cu-Mo deposit. It can be explained by weakly developed potassic and propylitic alteration zones, sub-economic Cu grades in the phyllic alteration zone, and geochemical characteristics of the granitoids (e.g., low to moderate Sr contents, moderate to high contents of Y and Yb, low to moderate ratios of Sr/Y and Dy/Yb, low La/Yb ratios, negative to slightly positive Eu anomalies, and negative anomalies of Sr).

Supplementary data to this article can be found online at https://doi.org/10.1016/j.gexplo.2019.01.001.

Acknowledgments

Professor P. Asimow at the California Institute of Technology, USA, is appreciated for English editing of the early version of the manuscript. Professor E.H. Christiansen at BYU is appreciated for his assistance with the analytical work. The authors express their gratitude to Dr. P. Davidson at ARC Centre of Excellence in Ore Deposits, University of Tasmania, Australia, for English editing of the final version of the manuscript. The authors acknowledg Professor Stefano Albanese, the Editor-in-Chief of Journal of Geochemical Exploration, and two anonymous reviewers for their critical comments and suggestions which helped greatly to improve the manuscript. The authors would like to thank the Research Council of Shiraz University for financial support of this work.

References

Aghazadeh, M., Hou, Z., Badrzadeh, Z., Zhou, L., 2015. Temporal-spatial distribution and tectonic setting of porphyry copper deposits in Iran: Constraints from zircon U-Pb and molybdenite Re-Os geochronology. Ore Geol. Rev. 70, 385–406.
Ahmadian, J., Haschke, M., Mcdonald, I., Regelous, M., Ghorbani, M.R., Emami, M.H., Murata, M., 2009. High magmatic flux during Alpine-Himalayan collision: constraints from the Kal-e-Kafi complex, central Iran. Geol. Soc. Am. Bull. 121, 857–868.
Almeida, M.E., Macambira, M.J.B., Oliveira, E.C., 2007. Geochemistry and zircon geochronology of the I-type high-K calc-alkaline and S-type granitoid rocks from southeastern Roraima, Brazil: Orosirian collisional magmatism evidence (1.97–1.96 Ga) in central portion of Guyana Shield. Precambrian Res. 155, 69–97.
Aminoroayaei Yamini, M., Tutti, F., Haschke, M., Ahmadian, J., Murata, M., 2017. Synorogenic Copper Mineralization During the Alpine-Himalayan Orogeny in the Zafarghand Copper Exploration District, Central Iran: Petrogrography, Geochemistry, and Alteration Thermometry.
Asadi, S., Moore, F., Zarasvandi, A., 2014. Discriminating productive and barren porphyry copper deposits in the southeastern part of the central Iranian volcano-plutonic belt, Kerman region, Iran. Earth Sci. Rev. 138, 25–46.
Ayati, F., Yavuz, F., Asadi, H.H., Richards, J.P., Jourdan, F., 2013. Petrology and geochemistry of calc-alkaline volcanic and subvolcanic rocks, Dalli porphyry copper-gold deposit, Markazi province, Iran. Int. Geol. Rev. 55, 158–184.
Batchelor, R.A., Bowden, P., 1985. Petrogenetic interpretation of granitoid rock series: using multinational parameters. Chem. Geol. 48, 43–55.
Berberian, F., Muir, I.D., Pankhurst, R.J., Berberian, M., 1982. Late Cretaceous and early Miocene Andean type plutonic activity in northern Makran and central Iran. J. Geol. Soc. (London, U.K.) 139, 605–614.
Borg, L.E., Clynne, M., 1998. The petrogenesis of felsic calc-alkaline magmas from the southernmost Cascades, California: Origin by partial melting of basaltic lower crust. J. Petrol. 39 (6), 1197–1222.
Brown, G.C., Thorpe, R.S., Webb, P.C., 1984. The geochemical characteristics of granitoids in contrasting arcs and comments on magma sources. J. Geol. Soc. Lond. 141, 413–426.
Chiu, H.Y., Chung, S.L., Zarrinkoub, M.H., Mohammadi, S.S., Khatib, M.M., Iizuka, Y., 2013. Zircon U-Pb age constraints from Iran on the magmatic evolution related to Neotethyan subduction and Zagros orogeny. Lithos 162-163, 70–87.
Condie, K.C., 2005. TTGs and adakites: are they both slab melts. Lithos 80, 33–44.
Davidson, J., Turner, S., Handley, H., Macpherson, C., Dosseto, A., 2007. Amphibole "sponge" in arc crust? Geology 35 (9), 787–790.
Defant, M.J., Drummond, M.S., 1990. Derivation of some modern arc magmas by melting of young subducted lithosphere. Nature 347, 662–665.
Defant, M.J., Jackson, T.E., Drummond, M.S., De Boer, J.Z., Bellon, H., Feigenson, M.D., Maury, R.C., Stewart, R.H., 1992. The geochemistry of young volcanism throughout western Panama and southeastern Costa Rica: an overview. J. Geol. Soc. (London, U.K.) 149, 569–579.
Dorsa Pardaze, 2012. Final Exploration Report from the Zefreh Copper Deposit (Unpublished report). pp. 128.
Drummond, M.S., Defant, M.J., Kepezhinskas, P.K., 1996. Petrogenesis of slab-derived trondhjemite-tonalite-dacite/adakite magmas. Earth Environ. Sci. Trans. R. Soc. Edinb. 87 (1–2), 205–215.
Foley, S., Tiepolo, M., Vannucci, R., 2002. Growth of early continental crust controlled by melting of amphibolite in subduction zones. Nature 417, 837–840.
Gavanji, N., 2010. Investigation on the Emplacement Mechanism of the South of Zafarghand (Ardestan) Granitoidic Pluton by AMS Method (Unpublished MSc. Thesis, MSc thesis). Shahrood University of Technology, Shahrood, Iran, pp. 223 (in Persian).
Ghasemi, A., Talbot, C.J., 2006. A new tectonic scenario for the Sanandaj-Sirjan zone, Iran. J. Asian Earth Sci. 26, 683–693.
Ghorbani, M.R., Graham, I.T., Ghaderi, M., 2014. Oligocene-Miocene geodynamic evolution of the central part of Urumieh-Dokhtar arc of Iran. Int. Geol. Rev. 56 (8), 1039–1050.
Gustafson, L.B., Hunt, J.P., 1975. The porphyry copper deposit at El Salvador, Chile. Econ. Geol. 70 (5), 857–912.
Henderson, P., 1984. Rare Earth Element Geochemistry. Elsevier, Amsterdam, pp. 510.
Hou, Z.Q., Duan, L.F., Lu, Y.J., Zheng, Y.C., Zhu, D.C., Yang, Z.M., Yang, Z.S., Wang, B.D., Pei, Y.R., Zhao, Z.D., McCuaig, T.C., 2015. Lithospheric architecture of the Lhasa Terrane and its control on ore deposits in the Himalayan-Tibetan orogeny. Econ. Geol. 110, 1541–1575.
Irvine, T.N., Baragar, W.R.A., 1971. A guide to the chemical classification of the common volcanic rocks. Can. J. Earth Sci. 8, 523–548.
Ishihara, S., 1977. The magnetite-series and ilmenite-series granitic rocks. Min. Geol. 27, 293–305.
Kay, R.W., Mahlburg-Kay, S., 1991. Creation and destruction of lower continental crust. Geol. Rundsch. 80 (2), 259–278.
Le Maitre, R.W., Streckeisen, A., Zanettin, B., Le Bas, M.J., Bonin, B., Bateman, P., 2002. Igneous Rocks: A Classification and Glossary of Terms, 2nd edition. Cambridge University Press, pp. 236.
Li, J.X., Qin, K.Z., Li, G.M., Xiao, B.X., Chen, L., Zhao, J.X., 2011. Post-collisional ore-bearing adakitic porphyries from Gangdese porphyry copper belt, southern Tibet: Melting of thickened juvenile arc lower crust. Lithos 126 (3), 265–277.
Lu, Y.J., Kerrich, R., Kemp, A.I.S., McCuaig, T.C., Hou, Z.Q., Hart, C.J.R., Li, Z.X., Cawood, P.A., Bagas, L., Yang, Z.M., Cliff, J., Belousova, E.A., Jourdan, F., Evans, N.J., 2013. Intracontinental Eocene-Oligocene porphyry Cu mineral systems of

Yunnan, western Yangtze Craton, China: Compositional characteristics, sources, and implications for continental collision metallogeny. Econ. Geol. 108, 1541–1576.
Lu, Y.J., Loucks, R.R., Fiorentini, M.L., Yang, Z.M., Hou, Z.Q., 2015. Fluid flux melting generated post-collisional high Sr/Y copper ore-forming water-rich magmas in Tibet. Geology 43, 583–586.
Martin, H., 1999. The adakitic magmas: Modern analogues of Archaean granitoids. Lithos 46 (3), 411–429.
McLemore, V.T., Munroe, E.A., Heizler, M.T., McKee, C., 1999. Geochemistry of the copper Flat porphyry and associated mining district, Sierra County, New Mexico, USA. J. Geochem. Explor. 67, 167–189.
Miyashiro, A., 1974. Volcanic rock series in island arcs and active continental margins. Am. J. Earth Sci. 274, 321–355.
Mohajjel, M., Fergusson, C.L., Sahandi, M.R., 2003. Cretaceous-Tertiary convergence and continental collision Sanandaj-Sirjan zone, western Iran. J. Asian Earth Sci. 21, 397–412.
Moyen, J.F., 2009. High Sr/Y and La/Yb ratios: the meaning of the “adakitic signature”. Lithos 112, 556–574.
Muir, R.J., Weaver, S.D., Bradshaw, J.D., Eby, G.N., Evans, J.A., 1995. The cretaceous separation point batholith, New Zealand: Granitoid magmas formed by melting of mafic lithosphere. J. Geol. Soc. 152, 689–701.
Müller, D., Rock, N.M.S., Groves, D.I., 1992. Geochemical discrimination between shoshonitic and potassic volcanic rocks in different tectonic settings: a pilot study. Mineral. Petrol. 46 (4), 259–289.
Mungall, E.J., 2002. Roasting the mantle: Slab melting and the genesis of major Au and Au-rich Cu deposits. Geology 30, 915–918.
Omrani, J., Agard, P., Whitechurch, H., Benoit, M., Prouteau, G., Jolivet, L., 2008. Arc magmatism and subduction history beneath the Zagros Mountains, Iran: a new report of adakites and geodynamic consequences. Lithos 106, 380–398.
Peccerillo, A., Taylor, S.R., 1976. Geochemistry of Eocene calc-alkaline volcanic rocks from the Kastamonu area, northern Turkey. Contrib. Mineral. Petrol. 58, 63–81.
Profeta, L., Ducea, M.N., Chapman, J.B., Paterson, S.R., Gonzales, S.M.H., Kirsch, M., Petrescu, L., DeCelles, P.G., 2015. Quantifying crustal thickness over time in magmatic arcs. Sci. Rep. 17786 (Nature Publishing Group).
Qiang, W., Zhenhua, Z., Jifeng, X., Xianhua, L., Zhiwei, B., Xiaolin, X., Yimao, L., 2003. Petrogenesis and metallogenesis of the Yanshanian adakite-like rocks in the eastern Yangtze block. Sci. China Ser. D Earth Sci. 46, 164–176.
Qin, K.Z., 2012. Preface for thematic articles “porphyry Cu-Au-Mo deposits in Tibet and Kazakhstan”. Resour. Geol. 62 (1), 1–3.
Radfar, J., Amini Chehragh, M.R., Emani, M.H., 1999. 1:100,000 geological map of the Ardestan. In: Geological Survey of Iran (GSI), Tehran.
Rapp, R.P., Shimizu, N., Norman, M.D., Applegate, G.S., 1999. Reaction between slab-derived melts and peridotite in the mantle wedge: experimental constraints at 3.8 GPa. Chem. Geol. 160, 335–356.
Rapp, R.P., Xiao, L., Shimizu, N., 2002. Experimental constraints on the origin of potassium-rich adakite in east China. Acta Petrol. Sin. 18, 293–311.
Richards, J.P., 2015. Tectonic, magmatic, and metallogenic evolution of the Tethyan orogen: from subduction to collision. Ore Geol. Rev. 70, 323–345.
Richards, J.P., Kerrich, R., 2007. Adakite-like rocks: their diverse origins and questionable role in metallogenesis. Econ. Geol. 102, 537–576.
Richards, J.P., Spell, T., Rameh, E., Razique, A., Fletcher, T., 2012. High Sr/Y magmas reflect arc maturity, high magmatic water content, and porphyry Cu ± Mo ± Au potential: examples from the Tethyan arcs of central and eastern Iran and western Pakistan. Econ. Geol. 107, 295–332.
Rossetti, F., Nasrabady, M., Theye, T., Gerdes, A., Monié, P., Lucci, F., Vignaroli, G., 2014. Adakite differentiation and emplacement in a subduction channel: the late Paleocene Sabzevar magmatism (NE Iran). Geol. Soc. Am. Bull. 126 (3–4), 317–343.
Salehi, T., Tangestani, M.H., 2018. Large-scale mapping of iron oxide and hydroxide minerals of Zefreh porphyry copper deposit, using Worldview-3 VNIR data in the northeastern Isfahan, Iran. Int. J. Appl. Earth Obs. Geoinf. 73, 156–169.
Sarjoughian, F., Kananian, A., 2017. Zircon U-Pb geochronology and emplacement history of intrusive rocks in the Ardestan section, central Iran. Geol. Acta 15, 25–36.
Sarjoughian, F., Lentz, D., Kananian, A., Ao, S., Xiao, W., 2018. Geochemical and isotopic constraints on the role of juvenile crust and magma mixing in the UDMA magmatism, Iran: evidence from mafic microgranular enclaves and cogenetic granitoids in the Zafarghand igneous complex. Int. J. Earth Sci. 107 (3), 1127–1151.
Shafiei, B., Haschke, M., Shahabpour, J., 2009. Recycling of orogenic arc crust triggers porphyry Cu mineralization in Kerman Cenozoic arc rocks, southeastern Iran. Mineral. Deposita 44, 265–283.
Shahabpour, J., 2005. Tectonic evolution of the orogenic arc in the region located between Kerman and Neyriz. J. Asian Earth Sci. 24, 405–417.
Sillitoe, R.H., 1972. A plate tectonic model for the origin of porphyry copper deposits. Econ. Geol. 67, 184–197.
Sillitoe, R.H., 2010. Porphyry copper systems. Econ. Geol. 105, 3–41.
Sun, S.S., McDonough, W.F., 1989. Chemical and isotopic systematics of oceanic basalts: Implications for mantle composition and processes. In: Saunders, A.D., Norry, M.J. (Eds.), Magmatism in Ocean Basins. Geol. Soc. London Spec. Publ 42. pp. 313–345.
Whitney, D.L., Evans, B.W., 2010. Abbreviations for names of rock-forming minerals. Am. Mineral. 95 (1), 185–187.
Yeganehfar, H., Ghorbani, M.R., Shinjo, R., Ghaderi, M., 2013. Magmatic and geodynamic evolution of Urumieh-Dokhtar basic volcanism, central Iran: Major, trace element, isotopic, and geochronologic Implications. Int. J. Earth Sci. 55 (6), 767–786.
Yin, J., Chen, W., Xiao, W., Yuan, C., Windley, B.F., Yu, S., Cai, K., 2017. Late Silurian-early Devonian adakitic granodiorite, A-type and I-type granites in NW Junggar, NW China: Partial melting of mafic lower crust and implications for slab roll-back. Gondwana Res. 43, 55–73.
Zarasvandi, A., Rezaei, M., Raith, J., Lentz, D., Azimzadeh, A.M., Pourkaseb, H., 2015. Geochemistry and fluid characteristics of the Dalli porphyry Cu-Au deposit, central Iran. J. Asian Earth Sci. 111, 175–191.